Autocatalytic Reaction Fronts Inside a Porous Medium of Glass Spheres

Severine Atis, Sandeep Saha, Harold Auradou, Dominique Salin, and Laurent Talon

Université Pierre et Marie Curie, 4 Place Jussieu, 75005 Paris, France and Université Paris-Sud, CNRS, Laboratoire FAST, Bâtiment 502, Campus Universitaire, Orsay F-91405, France

(Received 24 April 2012; revised manuscript received 10 September 2012; published 2 April 2013)

We analyze experimentally chemical wave propagation in the disordered flow field of a porous medium. The reaction fronts travel at a constant velocity that drastically depends on the mean flow direction and rate. The fronts may propagate either downstream and upstream but, surprisingly, they remain static over a range of flow rate values. Resulting from the competition between the chemical reaction and the disordered flow field, these frozen fronts display a particular sawtooth shape. The frozen regime is likely to be associated with front pinning in low velocity zones, the number of which varies with the ratio of the mean flow and the chemical front velocities.

DOI: 10.1103/PhysRevLett.110.148301 PACS numbers: 82.40.Ck, 47.54.−r, 82.33.Ln

Introduction.—Interface motion and front propagation are relevant to many processes, including chemical reactions [1], population dynamics in biology, flame propagation in combustion [2], and chemotaxis [3]. The dynamics of front propagation is well understood in stagnant fluids [4,5], whereas the effect of fluid flow on front motion is currently of immense interest [6–9]. In this experiment, we consider an autocatalytic reaction between two chemical species that generates a self-sustained reaction front [10,11]. These fronts propagate as solitary waves with a constant velocity ($V_\chi \propto \sqrt{D_m \alpha}$) and a stationary concentration profile of width ($l_\chi = D_m/V_\chi$), reflecting both the balance between molecular diffusion D_m and reaction rate α.

In heterogenous flow field, nonlinear coupling between reaction, diffusion, and advection generally induce long-range deformation of the reaction front. For instance, in a parabolic Poiseuille flow [7,12,13], this coupling leads to a stationary front concentration profile propagating at a constant velocity, whose shape and velocity are related to the local flow structure and the boundary conditions. More complex flows have been addressed with different nonlinear chemical reactions. In porous media, with a flow inside 10 mm diameter cylindrical tubes filled with glass beads [14,15], or in combined cellular flow and mean flow [9]. Interestingly, despite the differences in the flow nature and employed chemicals, both these experiments have echoed similar behaviors. Depending on the mean flow velocity and direction, the reaction fronts can travel downstream or upstream, but they can also remain static over a certain range of flow rate values. However, to our knowledge, there has been neither reaction front pattern formation observation nor freezing dynamics analysis in porous media. In this context, we have investigated the interaction of a self-sustained reaction front with the disordered flow field of a wide and transparent quasi—two-dimensional porous medium model. Our design allows the flow velocity fluctuation measurements and the direct observation of the reaction fronts. These experiments reveal new features on chemical wave propagation dynamics in disordered flow and pattern formation mechanisms.

In this Letter, we show visual aspects of frozen reaction fronts in the disordered flow of a porous medium. These static fronts are strongly distorted and display a remarkably straight sawtooth pattern, as shown in Fig. 1, the patterns aspect, the number of peaks and size, evolving with the mean flow rate. We determine the main characteristics of the flow field such as its correlation length and the spatiotemporal maps of the local velocities along the front as well as its probability distribution function (PDF). The patterns formation dynamics, correlated with the flow velocity fluctuations, leads then to a better physical understanding of the mechanisms at the origin of the frozen regime.

Experimental setup.—We performed experiments with the Iodate Arsenous Acid (IAA) autocatalytic reaction in iodide (I^-): $3H_3AsO_3 + IO_3^- + 5I^- \rightarrow 3H_3AsO_4 + 6I^-$.

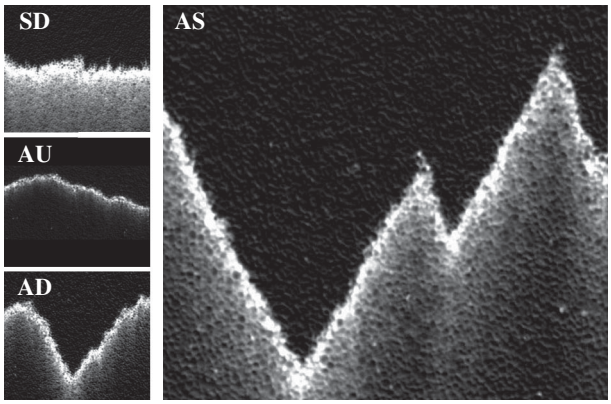

FIG. 1. Typical self-sustained chemical fronts in porous media. The first label corresponds to the mean flow direction, supportive S or adverse A to the chemical wave propagation; the second label denotes the front propagation direction, downstream D, upstream U, or static S.

For the concentration values used here ($[IO_3^-]_0 = 7.5$ mM, $[H_3AsO_3]_0 = 25$ mM), the arsenous is in excess [10]. The front position is localized by the transient generation of iodine during the reaction and marked by polyvinyl alcohol (see Fig. 1, for instance) [16].

The porous medium consists of a 50% mixture of 1.5 and 2 mm glass spheres (porosity: $48 \pm 2\%$). They are packed in a transparent rectangular cell ($30 \times 10 \times 1$ cm^3) as shown in Fig. 2. To overcome the buoyancy effect [17], we increase the viscosity to 10 mPa · s. The cell is filled with reactant solution and the chemical reaction is initiated at its bottom end. In the absence of flow, the reaction develops into a flat horizontal front propagating upward at the chemical velocity $V_\chi \simeq 10$ μm/s and $l_\chi \simeq 100$ μm. When the front reaches the desired vertical position, the flow is switched on and the fluid can be either sucked out or injected parallel to the vertical from the top of the cell. We extract the location $h(x)$ of the chemical pseudointerface at a given transverse distance x and define the front velocity by $v(x, t) = (h(x, t + \Delta t) - h(x, t))/\Delta t$; Δt is such that the variation of $h(x)$ is larger than the correlation length.

The net flow is characterized by its average value $\bar{U}$ and the characteristic length of the velocity fluctuation l_d is inferred from tracer dispersion experiments [18,19]: $l_d = (1.8 \pm 0.1)$ mm, which is close to the mean particle diameter, in agreement with Ref. [20]. Tracer front velocity fluctuations $u(x, t)$ are shown in Fig. 2. The spatiotemporal map displays the flow heterogeneities of characteristic size larger than l_d and the flow velocities PDF is asymmetric and well fitted by a log-normal distribution.

Front velocity.—We performed experiments over a wide range of mean flow velocities and measured the reaction front velocity. The fronts propagate with a velocity slightly fluctuating around a mean value, noted V_f. Counting as positive velocities in the direction of the reaction front propagation, $\bar{U} > 0$ corresponds to supportive flow (S) and $\bar{U} < 0$ to adverse flow (A). The mean front and mean flow velocities are, now, normalized by V_χ; $\bar{u} = \bar{U}/V_\chi$ and $v_f = V_f/V_\chi$. As can be seen from Fig. 3, v_f depends on both the value and direction of $\bar{u}$ and one can identify four different regimes of front propagation; the corresponding fronts' aspects are shown in Fig. 1. For supportive flow ($\bar{u} > 0$), the front propagates downstream, i.e., in the flow direction ($v_f > 0$). In this supportive downstream regime (SD), v_f varies almost linearly with $\bar{u}$ with a slope larger than 1. As demonstrated in Poiseuille flow [7,12], this may be attributed to the selection of the fastest streamline by the reaction front when propagating downstream. For adverse flow ($\bar{u} < 0$), the competition between the chemical wave and the flow field leads to more complex behaviors. For a small adverse flow rate $-1 \lesssim \bar{u} \lesssim 0$, the chemical wave overcomes the flow leading to upstream propagating fronts (AU, $v_f > 0$); v_f varies smoothly across the regimes SD and AU and approaches zero. The most salient regime is observed below $\bar{u} \simeq -1$. The reaction fronts are static without any fluctuations and display frozen sawtoothlike patterns (Fig. 1). They are observed over a range of mean flow velocities $\bar{u} \in [-3.2, -1]$, which corresponds to the plateau domain ($v_f = 0$, AS regime). Finally, for $\bar{u} \lesssim -3.2$, the flow is strong enough to overcome the chemical wave and so the front moves downstream, opposite to the chemical wave velocity ($v_f < 0$, AD). Its velocity varies again almost linearly with $\bar{u}$. However, in contrast to the SD regime, the resulting slope is smaller than 1, which is in agreement with similar experiments using Hele-Shaw cells [7].

Static fronts have been observed in Poiseuille flow in Hele-Shaw cells [7,12], but they were obtained only for a unique value of $\bar{u}$. In contrast, the velocity diagram determined here is similar to that observed in other contexts. For instance, the domains of observation of frozen fronts have been determined in combined cellular and mean opposite flow [9] as a function of the vortex and the mean adverse flow intensities. Static fronts in packed-bed reactors with different chemistries [14,15] have also been reported for adverse flow. Quite remarkably, the reaction fronts exhibit similar behaviors despite the important differences between these systems. Furthermore, one common feature

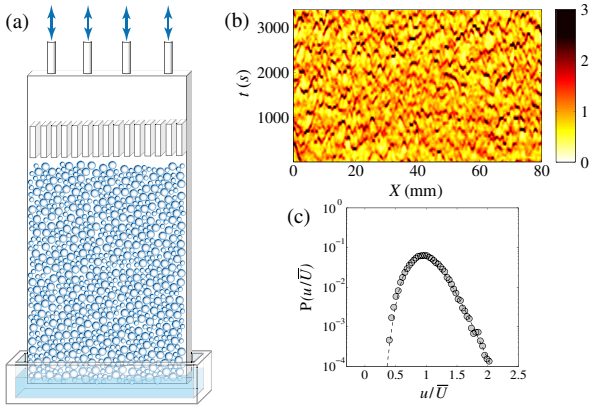

FIG. 2 (color online). (a) Experimental setup schematic. (b) Spatiotemporal map of the velocity variations measured with dye transport in the porous medium. (c) PDF of the above velocities' map (dots) and log-normal fit (dashed line).

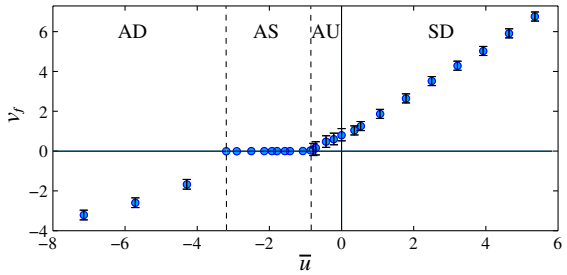

FIG. 3 (color online). Front velocity v_f versus mean flow velocity in the porous medium $\bar{u}$.

of all these experiments is the heterogeneity of the flow and shows here the key part the flow spatial structures play in frozen fronts formation.

Spatiotemporal dynamics.—One of the major motivations of these experiments is to understand how the flow velocity fluctuations alter the front propagation and account for the different regimes. This can be inferred from the front dynamics; Fig. 4 displays the spatiotemporal fluctuations of $v(x, t)$ and the associated PDFs in the different regimes. For *SD* fronts, the mean flow and the chemical wave are in the same direction; therefore, the measured local front velocities, $v(x, t)$ have positive values during the experiment. The PDF of these velocities has a log-normal shape with almost the same standard deviation as the one measured previously for the hydrodynamic flow field. This suggests that the hydrodynamic fluctuations dominate the front dynamic in this regime. The reaction front propagation is strikingly different in adverse flow regimes. The PDFs are modified indicating a more complex dynamical response than just the addition of the chemical velocity to the flow velocity distribution. Besides, they exhibit a local maximum at $v = 0$. This is a signature of transient static portions of fronts visible in white on the spatiotemporal maps. In the *AU* regime, the fronts propagate upstream; however, the large peak displayed on the PDF indicates the significance of zero velocity regions. When the front stops at a given location, it remains static until laterally traveling parts of the front reach these waiting regions. As a consequence, one can identify long-range lateral correlation of the velocities as dark regions on the spatiotemporal maps. They indicate the transversal propagation of the reaction at constant rate. In the *AS* regime, one can note that the final static pattern is achieved after a transient phase. Therefore, the spatiotemporal map describes the freezing dynamics of the front and the corresponding PDF is a transient distribution measured before the front stops. Velocity fluctuations are negative, illustrating the fact that the front is mostly pushed back by the flow until it pins locally to a pointlike region (at $X = 63$ mm in Fig. 4). The final front structure displays a sawtooth shape (Fig. 1), where each pinning point is at the vertex of a peak. However, before achieving the final pattern, transitorily pinned parts of the front are visible on the map as white stripes. In contrast to the *AU* regime, this demonstrates the long transversal correlation of zero velocity regions over time. Hence, the front partially pins several times during the whole experiment before it reaches an entirely frozen state. Finally, in the *AD* regime, fronts move downstream all along the experiments, and thus in this regime the flow seems to dominate the propagation of reaction. Yet a small peak at $v = 0$ on the PDF indicates the persistence of transitorily pinned parts of the fronts, but it progressively vanishes as the mean adverse flow velocity is increased.

Discussion.—The dynamical study has revealed pinning regions of the reaction fronts in adverse flows. They play a determining role in the freezing mechanism for the plateau regime (*AS*). Experiments on stationary Belousov-Zhabotinsky pulses have been reported in packed bead reactors [14] and linked to an "excited stagnant pockets" mechanism. When the reaction front reaches these regions, they act as a point source of chemical reaction. Producing and spreading catalyst, these pockets can sustain the reaction front in their vicinity. Although the chemical reaction is very different in that case, one can follow a similar argument in our experiments such that these pinning zones may correspond to stagnant flow pockets. However, this argument cannot account for reaction fronts moving downstream for sufficiently large adverse flow. This indicates that pinning points must be associated with weak but generally nonzero velocity zones, i.e., $-U(\vec{r}) \lesssim V_\chi$. Depinning of the front then occurs when the local flow velocity reaches a critical value that pushes the reaction out of this region. In this case, increasing the mean velocity results in reducing the number of low velocity zones

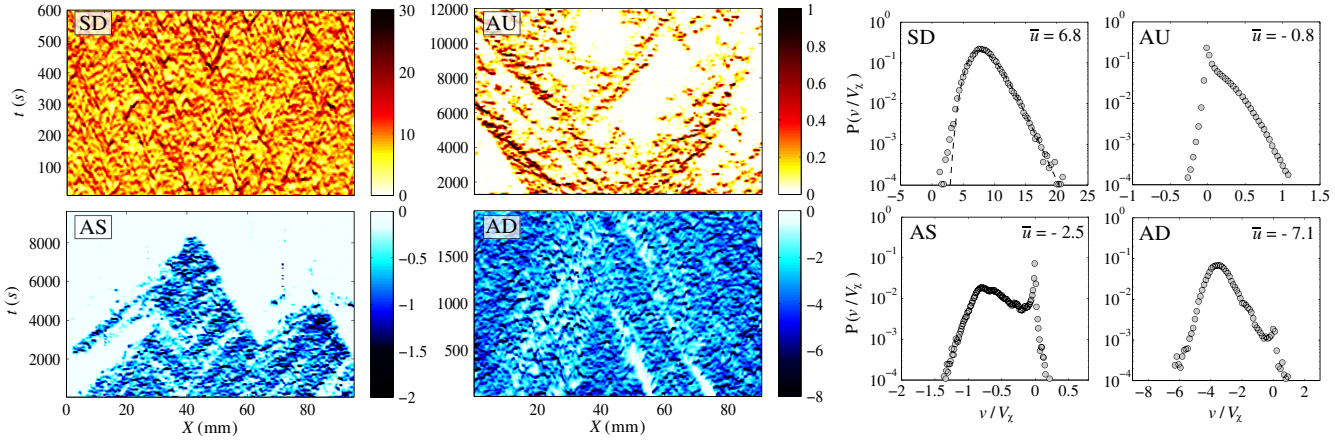

FIG. 4 (color online). Spatiotemporal representation of $v(x, t)$ for the four regimes. Color code intensity represents the magnitude of the velocity; red (top panels): $v > 0$, blue (bottom panels): $v < 0$. White regions correspond to $v = 0$. The corresponding PDFs of $v(x, t)$ (dots) and log-normal fit (dashed line).

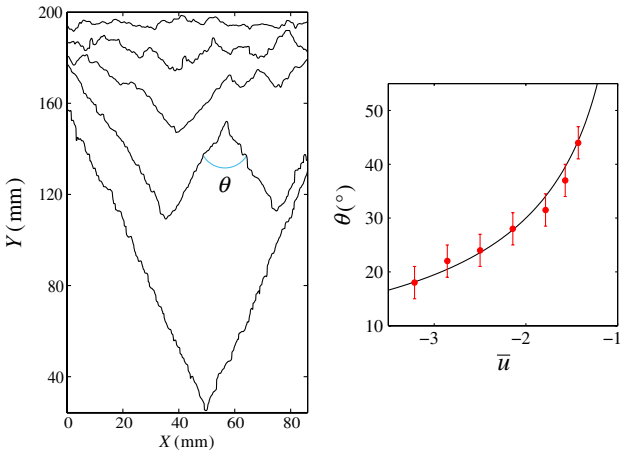

FIG. 5 (color online). Left: Frozen front aspects for different mean flow rate: from top to bottom, $\bar{u} = -1.4, -1.6, -1.9, -2.5, -3.2$. Right: Measurement of θ versus $\bar{u}$; solid line, theory.

required for pinning. One can note from the PDF on Fig. 2 that the minimal flow velocity value is $u_{\min} \sim 0.4\bar{U}$. One expects thus that the locations of this value act as pinning points as long as $-u_{\min} \lesssim V_\chi$ leading to a rough estimation of the transition at $\bar{u} \simeq -2.5$. This mechanism is supported by visual observations displayed on Fig. 5. Several frozen patterns recorded for different $\bar{u}$ values in the plateau domain are plotted and one can identify the location of the pinning points with the vertex of the front's peaks. Note that the two lateral boundaries can also be considered as pinning zones. As the flow velocity increases, the number of pinning points decreases until they vanish completely (except the two cell lateral boundaries) for $\bar{u} = -3.2$. This suggests that, statistically, the chemical reaction finds fewer pockets that can remain excited when $\bar{u}$ increases. The shapes of the final static fronts depend on the distribution of these pinning points but also on the initial location of the front.

Away from these zones, the flow velocity is much higher than V_χ, and yet the fronts reach a frozen state all over the porous medium. In order to understand these frozen fronts, one has to deal with the two flow regimes already analyzed in simple flows [7,12]. In the so-called mixing regime, the size of the flow extension (l_d) is much smaller than the chemical front width l_χ, and molecular diffusion has enough time to transversally mix the reactants leading to the Galilean invariance: $V_f = \bar{U} + V_\chi$. Therefore, static fronts are possible for a unique flow rate $\bar{U} = -V_\chi$; even with the flow distribution of Fig. 2, it is not enough to account for the plateau. In the opposite ($l_d \gg l_\chi$) thin front eikonal limit [21], at each point of the front surface, the normal component of the local interface velocity satisfies

$$\vec{V}_f(\vec{r}) \cdot \vec{n} = V_\chi + \vec{U}(\vec{r}) \cdot \vec{n} + D_m \kappa \qquad (1)$$

where $\vec{U}(\vec{r})$ is the local fluid velocity at the front position $\vec{r}$, $\vec{n}$ is the local unit vector normal to the interface, and κ the curvature of the interface. In this regime, frozen fronts can adjust their local inclination and curvature to accommodate larger local flow velocities and satisfy $V_f = 0$ in Eq. (1). Hence, increasing the flow intensity from $\bar{u} = -1$ to $\bar{u} = -3.2$ results in larger adverse flow leading to more inclination and bending of the front around pinning zones. Note that we are here in an intermediate regime ($l_d \sim 10 l_\chi$) where reactant concentration variations occur over a few l_χ; however, the thin front limit still explains the aspect of the frozen states. In Fig. 5, the teeth angle θ decreases with $|\bar{u}|$. Its value is in agreement with $V_\chi + \bar{U}\sin(\theta/2) = 0$ (solid line), which derives from Eq. (1) with the curvature term neglected on the straight parts of the front. Particularly, this pattern is analogous to the V shape displayed on flame fronts, strongly inclined in order to counterbalance high flow rate [22].

Finally, we have shown that the transient static portions of the fronts observed on the spatiotemporal maps correspond to transitory pinning zones that appears when approaching the plateau domain. During the experiments, the reaction fronts are temporally pinned at these locations. They form local static parts without leading to a completely frozen pattern and depin suddenly causing burstlike events. The irregular propagation of the fronts is hence due to successive rearrangements of the fronts when they travel from one low velocity zone to another one. In this configuration, the fronts propagate through local pinning and depinning events whose statistical properties [23] deserve further investigations aided by numerical simulations.

Conclusion.—We have experimentally investigated the propagation of chemical waves coupled to the disordered flow of a model porous medium. Depending on the mean flow direction and intensity, the reaction fronts exhibit four different regimes. Our experiments show the key role played by the flow heterogeneities on the chemical front dynamics. An interesting freezing regime is observed and explained by front pinning to low flow velocity regions. More specifically, we have analyzed the complex dynamic features involved in this pinning process. We thus expect that the domain of existence of this regime strongly depends on the flow heterogeneities distribution and further numerical simulations should be performed to analyze this dependence [24].

We thank J.-P. Hulin for stimulating discussions. The research was partly supported by CNES, RTRA "Triangle de la physique." S. S. was supported by the Initial Training Network (ITN) "Multiflow."

[1] S. K. Scott, *Oscillations, Waves, and Chaos in Chemical Kinetics*, Physical Vol. 18 (Oxford University, New York, 2004).
[2] Y. Zeldovich and D. Frank-Kamenetskii, Zh. Fi. Khim. **12**, 100 (1938).
[3] J. Adler, Science **153**, 708 (1966).

[4] R. Fisher, Ann. Eugenics **7**, 355 (1937).
[5] A. Kolmogorov, I. Petrovsky, and N. Piscounoff, Bull. Univ. Moscow, Ser. Int. A **1**, 1 (1937).
[6] M. Abel, A. Celani, D. Vergni, and A. Vulpiani, Phys. Rev. E **64**, 046307 (2001).
[7] B. F. Edwards, Phys. Rev. Lett. **89**, 104501 (2002).
[8] A. Pocheau and F. Harambat, Phys. Rev. E **73**, 065304 (2006).
[9] M. E. Schwartz and T. H. Solomon, Phys. Rev. Lett. **100**, 028302 (2008).
[10] A. Hanna, A. Saul, and K. Showalter, J. Am. Chem. Soc. **104**, 3838 (1982).
[11] A. Toth, D. Horvath, and A. Siska, J. Chem. Soc., Faraday Trans. **93**, 73 (1997).
[12] M. Leconte, J. Martin, N. Rakotomalala, and D. Salin, Phys. Rev. Lett. **90**, 128302 (2003).
[13] M. Leconte, N. Jarrige, J. Martin, N. Rakotomalala, D. Salin, and L. Talon, Phys. Fluids **20**, 057102 (2008).
[14] M. Kaern and M. Menzinger, J. Phys. Chem. B **106**, 3751 (2002).
[15] I. V. Koptyug, V. V. Zhivonitko, and R. Z. Sagdeev, J. Phys. Chem. B **112**, 1170 (2008).
[16] I. Bou Malham, N. Jarrige, J. Martin, N. Rakotomalala, L. Talon, and D. Salin, J. Chem. Phys. **133**, 244505 (2010).
[17] J. A. Pojman, I. R. Epstein, T. J. McManus, and K. Showalter, J. Phys. Chem. **95**, 1299 (1991).
[18] J.-P. Hulin and D. Salin, in *Disorder and Mixing*, edited by J. N. E. Guyon and Y. Pomeau (Kluwer Academic Publishers, Dordrecht, The Netherlands, 1988), Chap. 5.
[19] J. Bacri, N. Rakotomalala, and D. Salin, Phys. Rev. Lett. **58**, 2035 (1987).
[20] D. Koch and J. Brady, J. Fluid Mech. **154**, 399 (1985).
[21] F. Williams, in *Combustion Theory* (Benjamin/Cummings, New York, 1985), 2nd ed.
[22] T. Echekki and M. Mungal, Phys. Fluids A **2**, 1523 (1990).
[23] S. Santucci, R. Planet, K. J. Mly, and J. Ortn, Europhys. Lett. **94**, 46 005 (2011).
[24] S. Saha, S. Atis, D. Salin, and L. Talon, Europhys. Lett. **101**, 38 003 (2013).